Anisotropic vibrations in crystalline and amorphous InP

C. S. Schnohr, P. Kluth, L. L. Araujo, and D. J. Sprouster
Department of Electronic Materials Engineering, Research School of Physics and Engineering, The Australian National University, Canberra ACT 0200, Australia

A. P. Byrne
Department of Nuclear Physics, Research School of Physics and Engineering, The Australian National University, Canberra ACT 0200, Australia

G. J. Foran
Australian Nuclear Science and Technology Organisation, Menai NSW 2234, Australia

M. C. Ridgway
Department of Electronic Materials Engineering, Research School of Physics and Engineering, The Australian National University, Canberra ACT 0200, Australia

(Received 3 February 2009; published 5 May 2009)

The temperature-dependent evolution of atomic vibrations in crystalline and amorphous InP has been studied using extended x-ray absorption fine-structure (EXAFS) spectroscopy. Measurements were performed at the In *K* edge for temperatures in the range of 20–295 K. In crystalline InP, the first nearest-neighbor (NN) EXAFS Debye-Waller factor, representative of the *correlated* mean-square relative displacement (MSRD) parallel to the bond direction, is considerably smaller than the *uncorrelated* mean-square displacement (MSD) determined from x-ray diffraction measurements. In contrast, the MSRD perpendicular to the bond direction agrees well with the MSD. This clearly demonstrates that vibrations of two neighboring atoms relative to each other are strongly reduced along the bond direction but are unhindered perpendicular to it, consistent with the well-known behavior of III-V semiconductors where bond bending is energetically favored over bond stretching. With increasing interatomic distance, the correlation of atomic motion quickly vanishes as manifested by increased EXAFS Debye-Waller factors. For the third NN shell the value closely approaches the MSD demonstrating the nearly uncorrelated motion of atoms only three shells apart. In the amorphous phase, only information about the first NN shell is accessible although the latter is now comprised of both P and In atoms. The EXAFS Debye-Waller factors are significantly higher than in the crystalline phase but exhibit a very similar temperature dependence. This results from strongly increased *structural* disorder in the amorphous phase whereas the *thermally* induced disorder is very similar to that in crystalline InP. A correlated Einstein model was fitted to the Debye-Waller factors yielding Einstein temperatures that vary as functions of the vibrational phase difference and reduced mass of the atomic pair, and represent a measure of the strength and thermal evolution of the corresponding relative vibrations.

DOI: 10.1103/PhysRevB.79.195203 PACS number(s): 61.05.cj, 65.40.−b, 65.60.+a

I. INTRODUCTION

The temperature dependence of atomic motion in a solid contains information about vibrational and thermal properties such as force constants and Einstein or Debye temperatures. In contrast to x-ray diffraction (XRD), extended x-ray absorption fine-structure (EXAFS) spectroscopy is sensitive to the *correlated* motion of neighboring atoms and thus yields valuable insight into the phase relation of these vibrations. Furthermore, by comparing XRD and EXAFS measurements one can distinguish between vibrations parallel or perpendicular to the bond direction. Such knowledge provides an experimental test for phonon eigenvectors obtained from dynamical models or *ab initio* calculations.[1,2]

Beni and Platzman,[3] and Sevillano *et al.*[4] performed pioneering works for vibrational studies using temperature-dependent EXAFS measurements. The authors point out the difference between the *uncorrelated* mean-square displacement (MSD) sampled by XRD measurements and the *correlated* mean-square relative displacement (MSRD) obtained from EXAFS. They develop correlated Debye and Einstein models which take into account such correlations and, hence, are suitable to describe the temperature evolution of the measured EXAFS signal. Beni and Platzman[3] also discuss the effect of anisotropic vibrations in Zn, which has a hexagonal crystal structure, and use different directional Debye temperatures to describe the relative atomic motion along the different crystallographic directions.

Since then much effort has been devoted to establishing a well-founded relationship between the experimental parameters measured by EXAFS, and physical properties such as Debye and Einstein temperatures, force constants, and thermal-expansion coefficients.[1,5–11] Among the many systems studied are cubic metals,[2,7] monoelemental[8,12,13] and binary[14,15] semiconductors, and AgI.[1,16]

In an ideal Debye crystal, vibrations are isotropic and the ratio γ of the MSRD perpendicular to the bond to the MSRD parallel to the bond is two since the former describes vibrations in a plane while the latter denotes vibrations along a line. Furthermore, the MSRDs of all coordination shells are described by the same Debye temperature. Fornasini *et al.*[2] found γ for the first nearest-neighbor (NN) shell of Cu, a

monoelemental metal with the face-centered-cubic structure, to be between two and three, and thus close to the isotropic value. The Debye temperatures of the first four coordination shells were very similar with only the value for the second shell ~10–15 % lower as compared to the others. Cu thus closely resembles a perfect Debye crystal. For Ge, a monoelemental semiconductor with the diamond structure, γ of the first NN shell increases from ~3 at 10 K to ~5 at 300 K.[8] Furthermore, the MSRD along the line connecting the absorber-backscatterer pair is much higher for the second and third NN shells than for the first NN shell with the corresponding Einstein temperatures differing by a factor of two.[13] The latter is also the case for GaAs, a binary semiconductor with the zinc-blende structure.[14] This strikingly different behavior compared to Cu is attributed to the presence of optical modes in non-Bravais lattices and demonstrates the different extent to which atomic motion is correlated in the various coordination shells. CdSe (Ref. 15) and AgI (Ref. 1), both with a wurtzite structure and more ionic bonding character, have a first NN γ of ~13 and ~10, respectively. AgI also shows strong effects of anharmonicity even at room temperature.[1]

InP is both a technologically and scientifically interesting material. While it has the same crystal structure as GaAs, the two atomic constituents differ considerably relative to the materials discussed above: In has almost four times the mass of P, and approximately one and a half times the radius. Studying the vibrational properties of InP will thus complement the existing work, and will contribute to a better understanding of the mechanisms that lead to vibrational anisotropy and anharmonicity.

We have previously used EXAFS measurements at ~20 K to study the atomic-scale structure of InP amorphized by ion irradiation through either electronic or nuclear energy deposition.[17] Despite the fundamentally different energy-transfer mechanisms, no significant difference in the atomic structure was observed and a common process, namely, a quench from the melt, was considered responsible for amorphization in both energy regimes. In the present paper we report the results of temperature-dependent EXAFS measurements which reveal a striking anisotropy in the vibrational behavior of both crystalline (*c*-InP) and amorphous (*a*-InP) InP.

II. EXPERIMENTAL DETAILS

A powdered *c*-InP sample suitable for EXAFS transmission measurements was prepared by finely crushing a single-crystal InP wafer and mixing with BN. The amorphous InP phase was produced by ion irradiation with either electronic or nuclear energy deposition. To separate the material of interest from the bulk, InP/$In_{0.53}Ga_{0.47}As$/InP heterostructures [2.75 μm/50 nm/(100) substrate] were grown by metal organic chemical vapor deposition. For amorphization induced by electronic interaction [swift heavy-ion (SHI) sample] the material was irradiated at room temperature with 185 MeV Au ions to a fluence of 3×10^{13} cm^{-2}. The InP substrate and the $In_{0.53}Ga_{0.47}As$ layer were then removed by selective chemical etching. For amorphization due to nuclear energy deposition [low energy ion (LEI) sample] the material was irradiated at liquid nitrogen temperature with five different energies of Se ions ranging from 80 keV to 7 MeV and a total fluence of 8.5×10^{15} cm^{-2}. The InP substrate and the $In_{0.53}Ga_{0.47}As$ layer were removed by the same chemical processing but prior to irradiation. The amorphized InP films for both samples were then finely crushed and mixed with BN. Details of the sample preparation are given in Ref. 17.

EXAFS measurements of the In *K* edge (27.940 keV) were performed in transmission mode at beam line NW10A at the Photon Factory, Japan. Spectra were recorded at eight different temperatures ranging from 20 to 295 K. After the measurements, the SHI and LEI samples were annealed at 150 °C for 1 h then remeasured. Such low-temperature annealing leads to structural relaxation with the aim of achieving the intrinsic amorphous phase governed by the minimum-energy configuration.[18,19]

III. DATA ANALYSIS

A. Theoretical background

The well-established cumulant expansion method[5] enables the analysis of EXAFS measurements for slightly to moderately disordered systems in terms of the cumulants of the interatomic distance distribution: the first cumulant (R_{EXAFS}) corresponds to the mean value, the second cumulant or Debye-Waller factor ($\sigma^2_{\mathrm{EXAFS}}$) represents the standard deviation, and the third (C_3) and fourth (C_4) cumulants denote asymmetric and symmetric deviations from a Gaussian profile, respectively. Performing the analysis with the IFEFFIT approach (see Sec. III B) yields the cumulants of the *real* distance distribution and requires no corrections.[20] Nevertheless, EXAFS samples a one-dimensional distance distribution and care must be taken when comparing with three-dimensional atomic motion. Relations between the atomic displacement vectors and the cumulants are derived in detail in Refs. 2, 7, 8, and 10.

Since the EXAFS signal is the average over instantaneous interatomic distances, it is sensitive to the *correlated* motion of neighboring atoms. The EXAFS Debye-Waller factor, $\sigma^2_{\mathrm{EXAFS}}$, thus represents the *parallel* MSRD ($\mathrm{MSRD}_\parallel$), i.e., it is a measure for the vibrations of two atoms relative to each other along the bond direction for first NN atoms or along the line connecting the absorber-backscatterer pair for second and third NN atoms.[2,7] If $\mathbf{u}_0$ and $\mathbf{u}_j$ are the displacement vectors of absorber and backscatterer, respectively, then the $\mathrm{MSRD}_\parallel$ can be expressed as

$$\mathrm{MSRD}_\parallel = \langle[\hat{\mathbf{R}}\cdot(\mathbf{u}_j-\mathbf{u}_0)]^2\rangle = \langle(\hat{\mathbf{R}}\cdot\mathbf{u}_j)^2\rangle + \langle(\hat{\mathbf{R}}\cdot\mathbf{u}_0)^2\rangle - 2\langle(\hat{\mathbf{R}}\cdot\mathbf{u}_j)(\hat{\mathbf{R}}\cdot\mathbf{u}_0)\rangle, \quad (1)$$

where $\hat{\mathbf{R}}$ denotes the unit vector along the line connecting the absorber-backscatterer pair (see, for example, Fig. 5 in Ref. 7). $\mathrm{MSRD}_\parallel$ and thus $\sigma^2_{\mathrm{EXAFS}}$ do not contain information about vibrations *perpendicular* to the bond direction, i.e., the $\mathrm{MSRD}_\perp$, given by

$$\mathrm{MSRD}_\perp = \langle(\mathbf{u}_j-\mathbf{u}_0)(\mathbf{u}_j-\mathbf{u}_0)\rangle - \mathrm{MSRD}_\parallel. \quad (2)$$

Such information can, however, be obtained by comparing

the mean interatomic distance determined by EXAFS, R_{EXAFS}, with that obtained from XRD measurements, R_C. The latter represents the distance between the average atomic positions and is also known as the crystallographic distance. It has been shown that $R_{\mathrm{EXAFS}}=R_C+\mathrm{MSRD}_\perp/2R_0$, where R_0 denotes the interatomic distance in a state of absolute rest.[2,8] R_{EXAFS} is thus larger than R_C due to vibrations of the atoms perpendicular to the bond direction. In contrast to the MSRDs, the XRD Debye-Waller factor represents the MSD, i.e., the *uncorrelated* one-dimensional vibrations of two atoms averaged over all directions. For isotropic vibrations of the individual atoms, the sum of the first two terms in Eq. (1) corresponds to the MSD while the third term represents the *parallel* displacement correlation function.

The use of the correlated Debye model for non-Bravais crystals was shown to be questionable since the best fitting Debye temperatures for $\sigma^2_{\mathrm{EXAFS}}$ of the different NN shells vary significantly with respect to each other and to values obtained from other experimental techniques.[7] Furthermore, Vaccari and Fornasini[11] show that the derivation of the correlated Debye model for EXAFS MSRDs is not physically sound when applied to non-Bravais crystals. We therefore use the correlated Einstein model to analyze the temperature-dependent evolution of the MSRDs and MSDs. Treating the absorber-backscatterer pair as a one-dimensional oscillator and assuming an interaction potential of the form $V(r)=(1/2)k_0(r-r_0)^2-k_3(r-r_0)^3+\ldots$, where k_0 and k_3 are the harmonic and cubic force constants, respectively, the moments of the resulting distance distribution and their temperature dependence can be calculated (the pair-potential approach of Frenkel and Rehr,[6] and Yokoyama[9]). While the second and third moments correspond to the EXAFS second and third cumulants, the first moment calculated within this framework does not represent the EXAFS first cumulant due to the fact that the one-dimensional model cannot take into account the effect of perpendicular vibrations.[2] Therefore, only the relations for $\sigma^2_{\mathrm{EXAFS}}$ and C_3 will be used. In addition to the temperature-dependent terms, static contributions will be included to account for different configurations of structural disorder present in the various samples. Keeping only the lowest-order terms, the following relations are obtained[6,9]

$$\sigma^2_{\mathrm{EXAFS}}=\mathrm{MSRD}_\parallel=\frac{\hbar^2}{2\mu k_B}\frac{1}{E_\parallel}\coth\left(\frac{E_\parallel}{2T}\right)+\sigma^2_{\mathrm{static},\parallel}, \quad (3)$$

$$C_3=\frac{\hbar^6}{k_B^4\mu^3}\frac{k_3}{E_\parallel^4}\left\{\frac{3}{2}\left[\coth\left(\frac{E_\parallel}{2T}\right)\right]^2-1\right\}+C_{3,\mathrm{static}}. \quad (4)$$

Here T is the temperature, $\hbar$ and k_B denote Planck's constant divided by 2π and Boltzmann's constant, respectively, μ represents the reduced mass for the atomic pair, and $E_\parallel$ stands for the Einstein temperature with $E_\parallel=\hbar\omega_\parallel/k_B$. The Einstein frequency $\omega_\parallel$ is related to the harmonic force constant by $k_{0,\parallel}=\mu\omega_\parallel^2$. $\sigma^2_{\mathrm{static},\parallel}$ and $C_{3,\mathrm{static}}$ denote the static contributions which arise due to structural disorder. Equation (1) is also derived by Vaccari and Fornasini[11] using a three-dimensional approach for describing the MSRDs and approximating the phonon spectrum with a delta function at $\omega_\parallel$. Furthermore, they give a relation for the $\mathrm{MSRD}_\perp$ which only differs from Eq. (3) by a factor of two:

$$\mathrm{MSRD}_\perp=\frac{\hbar^2}{\mu k_B}\frac{1}{E_\perp}\coth\left(\frac{E_\perp}{2T}\right)+\sigma^2_{\mathrm{static},\perp}. \quad (5)$$

As the authors point out, there is no *a priori* reason why $E_\parallel$ and $E_\perp$ should be the same. For an isotropic crystal, however, one can assume that $E_\parallel=E_\perp$ and the ratio $\gamma=\mathrm{MSRD}_\perp/\mathrm{MSRD}_\parallel$ equals two.

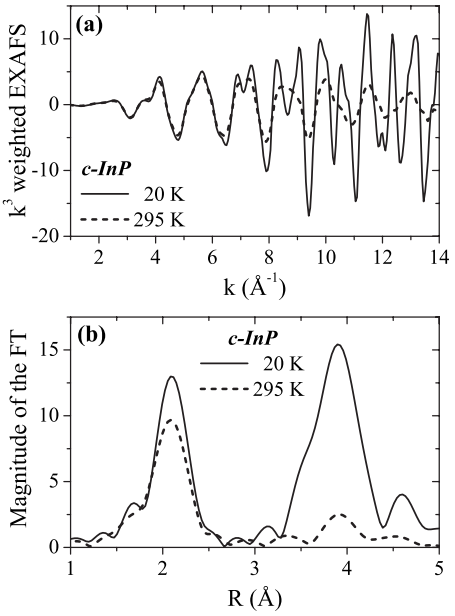

FIG. 1. (a) k^3-weighted EXAFS spectra of c-InP measured at 20 (solid line) and 295 K (dashed line) versus the photoelectron wave number k. (b) Corresponding Fourier transforms as a function of the nonphase-corrected radial distance R from the absorber.

B. Fitting procedure

The data were processed using the IFEFFIT code[21] and the corresponding user interface ATHENA.[22] After background removal, a Fourier transformation (FT) was performed over the photoelectron wave-number (k) range of $k=2-13.5$ Å^{-1}. Figures 1(a) and 2(a) show the k^3-weighted EXAFS as a function of k measured at 20 and 295 K for c-InP and a-InP (SHI relaxed), respectively. The corresponding FTs are plotted in Figs. 1(b) and 2(b). For c-InP, scattering from the first three NNs can be identified.[17] Interestingly, while the signal of the first peak in Fig. 1(b) (corresponding to first NN P atoms) is reduced by about 20% upon increasing the temperature from 20 to 295 K, the second (In) and third (P) NN peaks almost vanish. This clearly indicates a different thermal behavior for the different NN shells. For a-InP [Fig. 2(b)], only scattering from the first NN shell can be observed due to the increased disorder present in the amorphous phase. However, this shell is now comprised of both P and In atoms as apparent from the double-peak structure of the spectrum: scattering due to In-P and In-In pairs appears at $R\sim2.1$ Å and $R\sim2.6$ Å, respectively.[17] Increasing the measurement temperature leads to a decrease in the scatter-

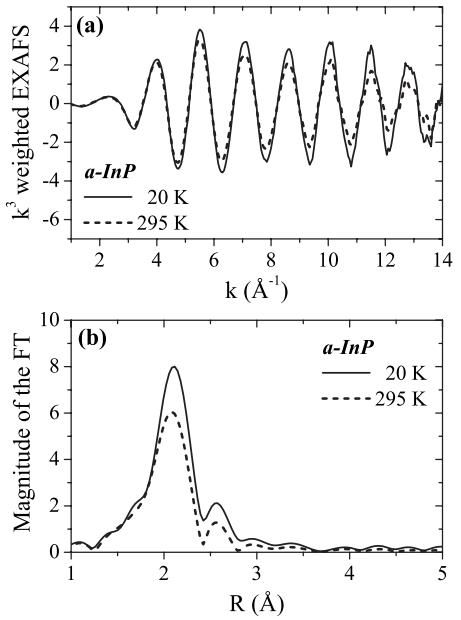

FIG. 2. (a) k^3-weighted EXAFS spectra of *a*-InP (SHI relaxed) measured at 20 (solid line) and 295 K (dashed line) versus the photoelectron wave number k. (b) Corresponding Fourier transforms as a function of the nonphase-corrected radial distance R from the absorber.

ing signal for both contributions with the drop for In-P being similar to that observed for *c*-InP.

The spectra were fitted in radial space with multiple k weights =2,3,4 over a range of $R=1.5-4.9$ Å using the IFEFFIT code[21] and the corresponding user interface ARTEMIS.[22] Scattering amplitudes and phase shifts were calculated *ab initio* with FEFF8 (Ref. 23) while the amplitude reduction factor (S_0^2) and the threshold energy (E_0) were determined from the crystalline sample, and then fixed throughout the analysis.[24]

For *c*-InP, the following parameters were determined from the fit for each of the measured temperatures: R_{EXAFS}, $\sigma^2_{\mathrm{EXAFS}}$, and C_3 for the first NN P and the second NN In paths while for the third NN P contribution only R_{EXAFS} and $\sigma^2_{\mathrm{EXAFS}}$ were floated. Due to the small signal and the overlap with the second NN peak, no temperature dependence could be extracted for the third NN C_3 and it was hence fixed to zero. The [In-In-P] multiple-scattering (MS) path was also included with its distance restrained by the distances of the first and second NN paths ($R^{(\mathrm{MS})}_{\mathrm{EXAFS}}=R^{(1)}_{\mathrm{EXAFS}}+R^{(2)}_{\mathrm{EXAFS}}/2$), and the Debye-Waller factor set equal to that of the second NN ($\sigma^{2(\mathrm{MS})}_{\mathrm{EXAFS}}=\sigma^{2(2)}_{\mathrm{EXAFS}}$). Tests were also performed with $\sigma^{2(\mathrm{MS})}_{\mathrm{EXAFS}}=\sigma^{2(2)}_{\mathrm{EXAFS}}/2$ and without including the MS path altogether corresponding to the two extreme cases of heavily overestimating or underestimating the influence of the MS path, respectively. None of the choices of how to treat the third NN path or the MS path had a significant influence on the first NN parameters or on the Debye-Waller factors of the higher shells. It did, however, strongly influence the second and third NN distances as well as $C_3^{(2)}$ and, thus, care has to be taken when interpreting these parameters. Furthermore, including a C_4 for the first NN path yielded values that were zero within uncertainty. Including C_4's for the higher shells will not result in physically meaningful values given the number of free parameters already present. Hence, fourth order cumulants were not further considered in the fitting procedure.

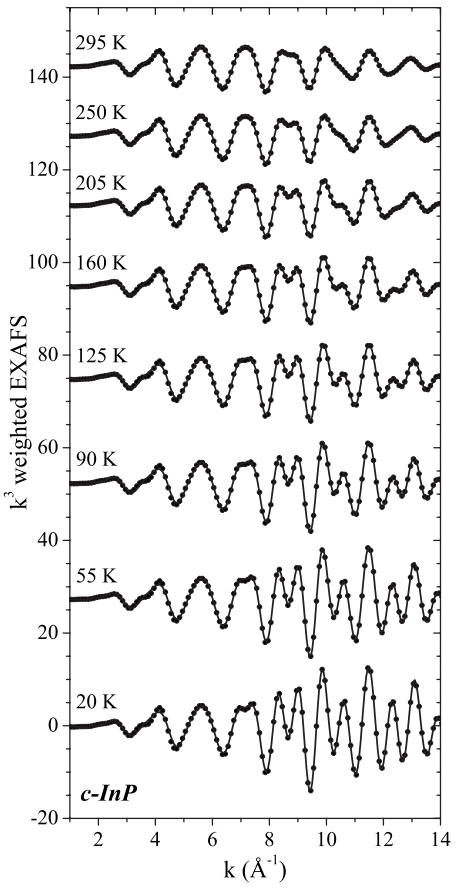

FIG. 3. k^3-weighted back-transformed experimental data (symbols) and best fits (lines) versus the photoelectron wave number k for *c*-InP. For clarity only every third data point is displayed and graphs for different temperatures are offset.

For *a*-InP, the coordination numbers for first NN P and In atoms were fixed to the values previously obtained for the as-irradiated and relaxed SHI and LEI samples.[17] During the fit at each temperature, separate R_{EXAFS} and $\sigma^2_{\mathrm{EXAFS}}$ were floated for both contributions while a C_3 was only included for In-P. Given the comparatively weak In-In signal compounded by overlap with the In-P peak, no temperature dependence could be rightfully extracted for an In-In C_3. However, in amorphous materials a positive C_3 is to be expected even at low temperatures. Thus for consistency a constant C_3 was included for In-In, determined from the 20 K spectrum and then fixed for all other temperatures. Fits are shown in Figs. 3 and 4 for *c*-InP and *a*-InP (SHI relaxed), respectively, together with the back-transformed experimental data. Clearly, fit and data are in excellent agreement for all temperatures. The fits for the other three *a*-InP samples (not shown) were of similar quality.

To minimize the number of free parameters, we did not include C_3's in our previous study.[17] Having now fixed the coordination numbers herein, we reintroduce C_3's with the knowledge that these amplitude- and phase-dependent pa-

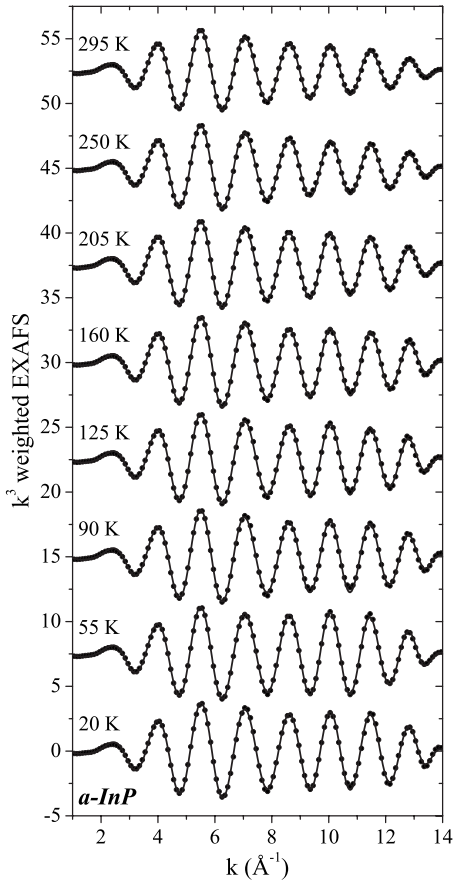

FIG. 4. k^3-weighted back-transformed experimental data (symbols) and best fits (lines) versus the photoelectron wave number k for a-InP (SHI relaxed). For clarity only every third data point is displayed and graphs for different temperatures are offset.

rameters (coordination number and C_3, respectively) are not strongly correlated. The inclusion of C_3's can, however, influence the other phase-dependent parameter (the interatomic distance), and thus Table I lists the first NN structural parameters of c-InP and a-InP measured at 20 K as obtained in the present study. Compared with the values given in Ref. 17, slight differences in bond length are apparent as expected. In no way do such differences alter our previous conclusion that there is no significant difference in the atomic structure of SHI and LEI a-InP samples.

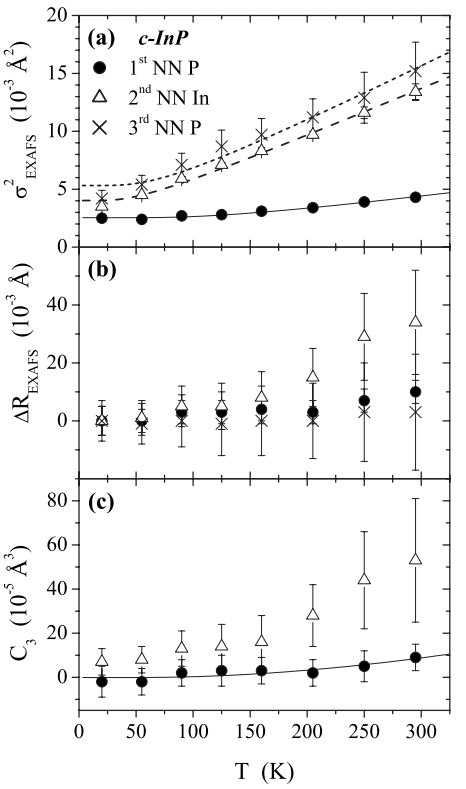

FIG. 5. (a) Debye-Waller factor $\sigma^2_{\mathrm{EXAFS}}$, (b) interatomic distance $\Delta R_{\mathrm{EXAFS}}=R_{\mathrm{EXAFS}}(T)-R_{\mathrm{EXAFS}}(T=0\ \mathrm{K})$, and (c) third cumulant C_3 versus temperature T for c-InP. Values are given for first NN P (full circles), second NN In (open triangles), and third NN P (crosses) atoms. The lines show the corresponding fits with the Einstein model (see Secs. III A and IV A).

IV. RESULTS AND DISCUSSION

A. Crystalline InP

Figure 5 shows the temperature dependence of all fitting parameters determined for c-InP. The Debye-Waller factor $\sigma^2_{\mathrm{EXAFS}}$ [Fig. 5(a)] increases with both temperature and distance of the absorber-backscatterer pair. Strikingly, the values for the second and third NN shells are significantly higher than the first NN ones, reflecting differences in the thermally induced amplitude reduction for these shells. Similar behavior has been observed for Ge,[13] GaAs,[14] and AgI.[16]

TABLE I. First NN structural parameters for c-InP and a-InP measured at a temperature of 20 K. The latter was amorphized by either 185 MeV Au irradiation (SHI) or by multiple-energy Se irradiation in the range of 0.08–7 MeV (LEI). The coordination number (N), bond length (R_{EXAFS}), Debye-Waller factor ($\sigma^2_{\mathrm{EXAFS}}$), and third cumulant ($C_3$) are listed for the first shell In-P and In-In pairs.

		First NN In-P				First NN In-In			
		N	R_{EXAFS} (Å)	$\sigma^2_{\mathrm{EXAFS}}$ (10^{-3} Å^2)	C_3 (10^{-5} Å^3)	N	R_{EXAFS} (Å)	$\sigma^2_{\mathrm{EXAFS}}$ (10^{-3} Å^2)	C_3 (10^{-5} Å^3)
c-InP		4	2.541 ± 0.005	2.5 ± 0.2	-2 ± 7				
a-InP SHI	As-irrad	3.43	2.584 ± 0.003	5.6 ± 0.2	22 ± 7	0.70	2.799 ± 0.006	5.8 ± 0.5	10 ± 20
	Relaxed	3.54	2.576 ± 0.003	5.0 ± 0.2	16 ± 6	0.66	2.796 ± 0.006	5.8 ± 0.5	20 ± 20
a-InP LEI	As-irrad	3.47	2.584 ± 0.003	5.8 ± 0.2	19 ± 6	0.63	2.813 ± 0.004	4.4 ± 0.3	30 ± 20
	Relaxed	3.57	2.580 ± 0.002	5.3 ± 0.2	18 ± 5	0.57	2.808 ± 0.004	4.4 ± 0.3	30 ± 20

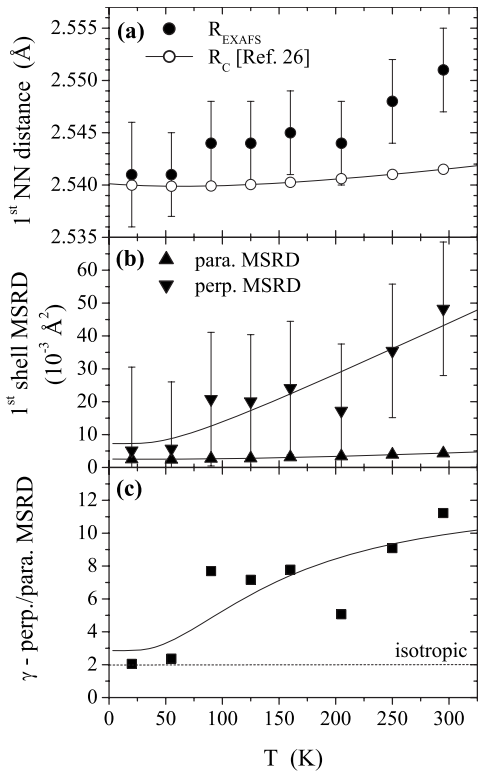

FIG. 6. (a) First NN distance of *c*-InP determined from EXAFS, R_{EXAFS} (full circles), and from XRD, R_C (open circles), versus temperature T. (b) Parallel (up triangles) and perpendicular (down triangles) MSRDs as a function of T for the first NN shell of *c*-InP. The solid lines show the corresponding Einstein fits. (c) Ratio γ of perpendicular to parallel MSRD for the data points (squares) and the fits (line) given in panel (b).

$\Delta R_{EXAFS}[R_{EXAFS}(T)-R_{EXAFS}(T=0\ \mathrm{K})]$ and C_3 for the first NN P slightly increase with temperature. For the second NN In, they both increase with temperature more rapidly than the first NN values for all fitting protocols.[25] The nearly constant ΔR_{EXAFS} for third NN P is not physically meaningful without including a temperature-dependent C_3. We contend that our choice of not including a C_3 for the third NN shell altogether (rather than having a constant nonzero value) is justified given that C_3 is approximately zero at low temperature for both first and second NNs.

Figure 6(a) shows the first NN distance determined from EXAFS, R_{EXAFS}, and the corresponding values obtained from XRD measurements,[26] R_C, as a function of temperature T. Two observations are readily apparent: (i) R_{EXAFS} is larger than R_C at all temperatures and (ii) the difference increases with increasing temperature. As noted in Sec. III A, this difference results from vibrations perpendicular to the bond direction. The increase in R_C with temperature is caused only by the anharmonicity of the crystal potential while the increase in R_{EXAFS} is also due to the increase in vibrational motion at higher temperatures.

Figure 6(b) plots for first NN P the $MSRD_\perp$ determined from the values shown in Fig. 6(a) together with the $MSRD_\parallel=\sigma^2_{EXAFS}$. The $MSRD_\perp$ is larger than the $MSRD_\parallel$ and increases more rapidly with temperature. The ratio $\gamma=MSRD_\perp/MSRD_\parallel$, plotted in Fig. 6(c), is close to the isotropic value of two at low temperatures, increasing to approximately ten at room temperature. This value is significantly higher than that of ~5 reported for Ge (Ref. 8) but very similar to the values of ~13 and ~10 determined for CdSe (Ref. 15) and AgI (Ref. 1), respectively. One can therefore distinguish three groups: (i) Cu (Ref. 2) with γ close to the isotropic value of two, (ii) Ge which already exhibits vibrational anisotropy, and (iii) InP, CdSe, and AgI with the highest values of γ. The latter three materials behave similarly despite their different crystal structures, and different ratios of mass and electronegativity of their atomic constituents. Significant vibrational anisotropy is thus present in the materials studied with a non-Bravais lattice structure. Furthermore, it is more pronounced for the binaries compared to monoelemental Ge.

As noted by Fornasini *et al.*,[2] the main contribution to the third cumulant C_3 comes from the anharmonicity of the crystal potential. InP, CdSe (Ref. 15), and Cu (Ref. 2) all show very similar values for C_3 ranging from 9 to 15×10^{-5} Å^3 at room temperature. For Ge, a slightly lower value of 3×10^{-5} Å^3 has been reported.[8,20] In contrast, AgI exhibits much greater anharmonicity, with $C_3\sim80\times10^{-5}$ Å^3.

The degree of correlation governing the motion of the different NN shells becomes apparent when comparing the EXAFS MSRDs to the MSDs determined by XRD. Following Böhmer and Rabe,[27] the one-dimensional MSD has been calculated by $MSD_{In+P}=(B_{In}+B_P)/8\pi^2$ and $MSD_{In+In}=(B_{In}+B_{In})/8\pi^2$ for In-P and In-In pairs, respectively, where B_{In} and B_P are the XRD Debye-Waller factors for In and P atoms, respectively. Experimental XRD B values of InP are reported for room temperature by Saravanan *et al.*[28] while Reid[29] calculated B values for a variety of zinc-blende materials over a large temperature range. Schowalter *et al.*[30] recently computed and parametrized the MSD temperature dependence for group IV, III-V, and II-VI semiconductors. The values are shown in Figs. 7(a) and 7(b) for In-P and In-In pairs, respectively. Also plotted are the first NN $MSRD_\parallel$ and $MSRD_\perp/2$, and the third NN $MSRD_\parallel$ in panel (a). The second NN $MSRD_\parallel$ is shown in panel (b). Since all MSDs and $MSRD_\parallel$s represent atomic motion along a line, the factor of one half must be used for the $MSRD_\perp$ (which describes atomic motion in a plane) when comparing one another.

Considering the first NN shell [Fig. 7(a)], it is now evident that the $MSRD_\parallel$ is much smaller than the MSD while the $MSRD_\perp/2$ is very similar. The MSD values reported by Schowalter *et al.*[30] were calculated based on the assumption that thermal vibrations of individual atoms are isotropic. The sum of the first two terms in Eq. (1) thus corresponds to the MSD, and a smaller $MSRD_\parallel$ is only possible if the absorber and backscatterer vibrations along the bond direction are at least partially *in phase* resulting in a positive displacement correlation function [third term in Eq. (1)]. Following Sanson *et al.*,[31] the $MSRD_\parallel$ for the extreme case of vibrations perfectly in phase has been calculated using the MSD values by Schowalter *et al.*[30] and amounts to 0.04×10^{-3} Å^2 at 295 K. This value is significantly smaller than the measured $MSRD_\parallel=4.3\pm0.2\times10^{-3}$ Å^2. The difference between MSD and $MSRD_\parallel$ values is thus consistent with a strong (but not complete) in-phase motion of the neighboring atoms along the bond direction. In contrast, the similarity between MSD

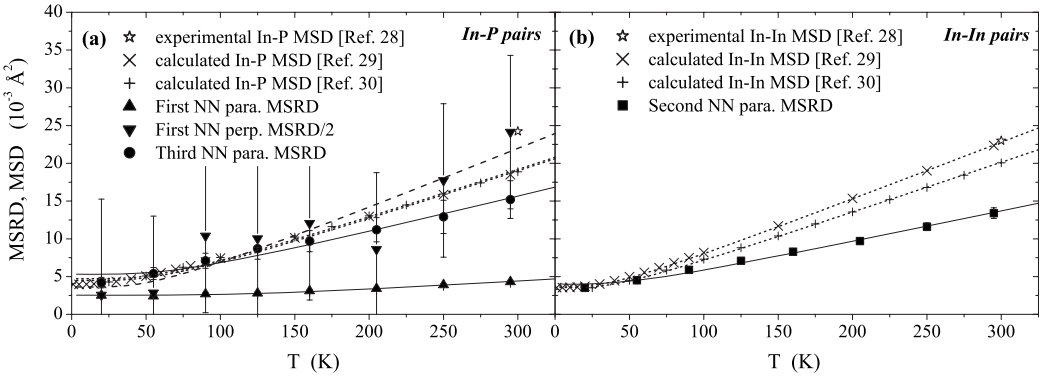

FIG. 7. MSDs and MSRDs for (a) In-P and (b) In-In pairs of *c*-InP. The MSD values were calculated from the data reported by Saravanan *et al.* (Ref. 28) (open stars), Reid (Ref. 29) (× crosses), and Schowalter *et al.* (Ref. 30) (+ crosses). $MSRD_{\parallel}$ and $MSRD_{\perp}/2$ for the first NN shell are given in panel (a) by full up and down triangles, respectively. Second NN $MSRD_{\parallel}$ are plotted as full squares in panel (b) and third NN $MSRD_{\parallel}$ are shown as full circles in panel (a).

and $MSRD_{\perp}/2$ indicates that the vibrations perpendicular to the bond direction are uncorrelated since the last term in Eq. (1) has to vanish. This behavior is further illustrated by the Einstein temperatures E given in Table II that were obtained from best fits of the data with Einstein models (1) and (3) [see Sec. III A and Figs. 5–7]. While relative vibrations parallel to the bond direction are characterized by $E_{\parallel}^{(1)}=392\pm8$ K, the value for relative vibrations perpendicular is $E_{\perp}^{(1)}=160\pm20$ K in good agreement with $E=174\pm2$ K for the MSD. To our knowledge, no direct measurement of the Einstein temperature for InP has been reported. Debye temperatures published in the literature range from 210 to 440 K depending on the temperature and method of determination.[32,33] Einstein temperatures reported for the EXAFS first NN $MSRD_{\parallel}$ of Ge range from 350 to 360 K (Refs. 8, 13, and 20) while that for GaAs is $E_{\parallel}^{(1)}=360\pm20$ K.[14]

Although the significant difference between relative vibrations parallel and perpendicular to the bond direction may at first seem surprising, it is entirely consistent with the well-known behavior of III-V semiconductor ternary alloys where the lattice mismatch of the binary compounds is accommodated primarily by bond angle relaxation and to a much lesser extent by bond-length relaxation (see Ref. 34 and references therein). Bond bending is thus energetically much more favorable than bond stretching. Since relative vibrations parallel to the bond require bond stretching whereas relative vibrations perpendicular to the bond mainly involve bond bending, the observed vibrational anisotropy can be easily understood.

Many of the models that describe the structural distortions in ternary alloys use the Keating potential[35] which consists of bond-stretching and bond-bending terms. The corresponding force constants α and β are deduced from fitting experimental bulk moduli and elastic constants.[36,37] Considering only the bond stretching term for a single bond and comparing the coefficient of the harmonic contribution with the potential given in Sec. III A, it follows that $k_{0,\parallel}^{(1)}=3\alpha$. Our value of $k_{0,\parallel}^{(1)}=107\pm4$ N m^{-1} indeed agrees reasonably well with the values of $3\alpha=129$ N m^{-1} and $3\alpha=121$ N m^{-1} reported by Martin,[36] and Chen and Sher,[37] respectively. Furthermore, the ratio of parallel to perpendicular force constants determined herein, $k_{0,\parallel}^{(1)}/k_{0,\perp}^{(1)}\sim6$, agrees well with the ratio of bond-stretching to bond-bending force constants, $\alpha/\beta\sim7$ and $\alpha/\beta\sim6$, reported in Refs. 36 and 37, respectively. The strong vibrational anisotropy observed for InP in this study is clearly related to the difference in energy required for bond bending and bond stretching in III-V semiconductors with the zinc-blende structure.

Comparing the $MSRD_{\parallel}$ of the first three NN shells with the corresponding MSDs [Fig. 7(a) for In-P pairs and Fig. 7(b) for In-In pairs], we observe the following: (i) the first NN $MSRD_{\parallel}$ is significantly smaller than MSD_{In+P} due to a strong correlation of the first NN atomic motion as discussed above. (ii) The second NN $MSRD_{\parallel}$ is considerably larger than that of the first NN but still significantly lower than MSD_{In+In} whereas (iii) the third NN $MSRD_{\parallel}$ approaches the MSD_{In+P} values. The degree of correlation governing the atomic motion thus decreases rapidly with increasing distance between the absorber-backscatterer pair. Correspondingly, the difference between the Einstein temperatures for $MSRD_{\parallel}$ and MSD decreases with increasing scattering distance. A similar observation was reported for GaAs where the third NN $MSRD_{\parallel}$ agrees well with the corresponding

TABLE II. Einstein temperature E and static contribution to the Debye-Waller factor σ_{static}^2 as determined from fits with a correlated Einstein model for *c*-InP.

		E(K)	σ_{static}^2 (10^{-3} Å^2)
In-P	MSD_{In+P} [a]	174 ± 2	−1.2 ± 0.2
	MSD_{In+P} [b]	174 ± 2	−1.0 ± 0.2
	First NN $MSRD_{\parallel}$	392 ± 8	0.0 ± 0.2
	First NN $\frac{1}{2}MSRD_{\perp}$	160 ± 20	−3 ± 10
	Third NN $MSRD_{\parallel}$	200 ± 10	0.4 ± 0.7
In-In	MSD_{In+In} [a]	105 ± 1	−0.3 ± 0.1
	MSD_{In+In} [b]	112 ± 1	−0.2 ± 0.1
	Second NN $MSRD_{\parallel}$	143 ± 5	1.1 ± 0.2

[a]Reference 29.
[b]Reference 30.

MSD.[14] Note that for GaAs the Einstein temperatures decrease continually with increasing NN distance while for InP the second NN value is smaller than that of the third NN, $E_{\parallel}^{(2)}=143\pm5<E_{\parallel}^{(3)}=200\pm10$, due to the large difference in reduced mass μ for In-P and In-In pairs (negligible for GaAs).

The decrease in correlated motion for the higher shells is consistent with the lack of physical bonds between the absorber and second or third NNs. A change in first NN distance requires energetically unfavorable bond stretching. In contrast, a change in second or third NN distance can be achieved by bond bending at the bridging atom without changing first NN bond lengths. Additional bridging atoms thus make it more likely that energetically favored bond bending will lead to a change in the corresponding higher NN distance. Hence, the correlation of vibrations along the absorber-backscatterer line strongly decreases for the higher shells and already approaches the MSD for the third NN shell (two bridging atoms).

B. Amorphous InP

In contrast to the crystalline phase of InP which comprises only heteropolar bonds (In-P), the amorphous phase contains both heteropolar and homopolar bonds (In-P and In-In around In atoms, respectively). Figures 8 and 9 show the temperature dependence of the structural parameters determined for first NN P and In atoms, respectively. Values are given for the as-irradiated and relaxed SHI and LEI samples. For the P contribution (Fig. 8), the parameters of *c*-InP are also included for comparison. Table III summarizes the parameters obtained from the corresponding best fits using Eqs. (1) and (2). The EXAFS Debye-Waller factor for the first NN In-P pairs [Fig. 8(a)] for all amorphous samples is much higher than the crystalline values but with a similar temperature dependence. $\sigma^2_{\mathrm{EXAFS}}$ for the LEI and SHI samples are very similar with the values of the relaxed phase slightly lower than those of the as-irradiated state. This behavior is reflected by the parameters determined from the Einstein fits: $E_{\parallel}^{(\mathrm{In-P})}\sim390$ K for *c*-InP, ~370 K for as-irradiated *a*-InP, and ~380 K for relaxed *a*-InP. A slightly lower Einstein temperature of the amorphous phase compared to that of the crystalline phase has also been reported for Ge (330 ± 10 K and 360 ± 10 K, respectively) (Ref. 13) and is consistent with slightly looser or floppier bonds in the amorphous material. The static contribution is zero for *c*-InP whereas $\sigma^{2(\mathrm{In-P})}_{\mathrm{static},\parallel}\sim3\times10^{-3}$ Å^2 for *a*-InP. Hence, *thermally* induced disorder is very similar for *c*-InP and *a*-InP while *structural* disorder is clearly much higher in the amorphous phase.

The other In-P parameters yield similar findings [Figs. 8(b) and 8(c), respectively]: (i) $\Delta R_{\mathrm{EXAFS}}$ values are very similar for all amorphous samples (with the relaxed values slightly lower than those for the as-irradiated samples) but significantly higher than the crystalline values. The latter is typical for semiconductors[38,39] and is consistent with sampling more anharmonicity of the interaction potential due to increased disorder in the amorphous phase. For both *a*-InP and *c*-InP, the temperature dependence of $\Delta R_{\mathrm{EXAFS}}$ is slight. (ii) C_3 values of all *a*-InP samples are very similar and significantly higher than that of *c*-InP. Nevertheless, both phases show approximately the same temperature dependence as confirmed by the k_3 values given in Table III which agree within experimental uncertainty. In contrast, the static contribution to the third cumulant is zero within uncertainty for *c*-InP but ranges from $19\times10^{-5}-25\times10^{-5}$ Å^3 for *a*-InP.

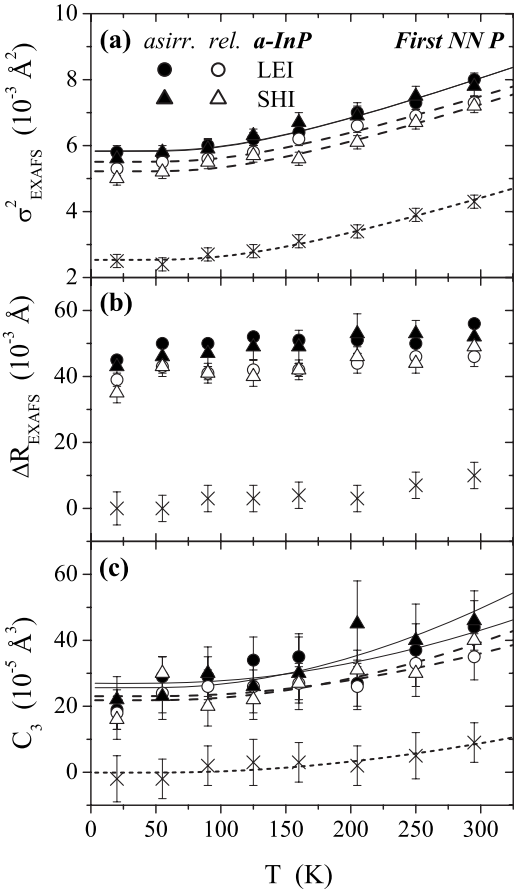

FIG. 8. (a) Debye-Waller factor $\sigma^2_{\mathrm{EXAFS}}$, (b) interatomic distance $\Delta R_{\mathrm{EXAFS}}=R_{\mathrm{EXAFS}}(T)-2.541$ Å, and (c) third cumulant C_3 versus temperature T for first NN P in *a*-InP. LEI and SHI samples are plotted as circles and triangles, respectively. Full symbols represent the as-irradiated phase whereas open symbols give the parameters obtained after relaxation. The values for *c*-InP are also included for comparison (crosses). The lines show the corresponding Einstein model fits.

No comparison with *c*-InP is possible for the first NN In contribution (Fig. 9) since homopolar bonds do not exist in the crystalline zinc-blende phase. The different *a*-InP samples have comparable $\sigma^2_{\mathrm{EXAFS}}$ values in as-irradiated and relaxed states, and are slightly higher for the SHI sample as addressed in our previous low-temperature study.[17] The first NN In-In distances are similar and appear roughly constant with temperature for all amorphous samples although the temperature evolution of $\Delta R_{\mathrm{EXAFS}}$ is not physically meaningful without a temperature-dependent C_3 included in the fit. The C_3 values determined for the four a-InP samples at $T=20$ K agree within experimental uncertainty [see Table I].

Comparing the Einstein temperatures $E_{\parallel}$ of the amorphous samples with those of *c*-InP MSD and MSRD$_{\parallel}$ is instructive. Despite the subtle differences of the $E_{\parallel}$ values given for In-P

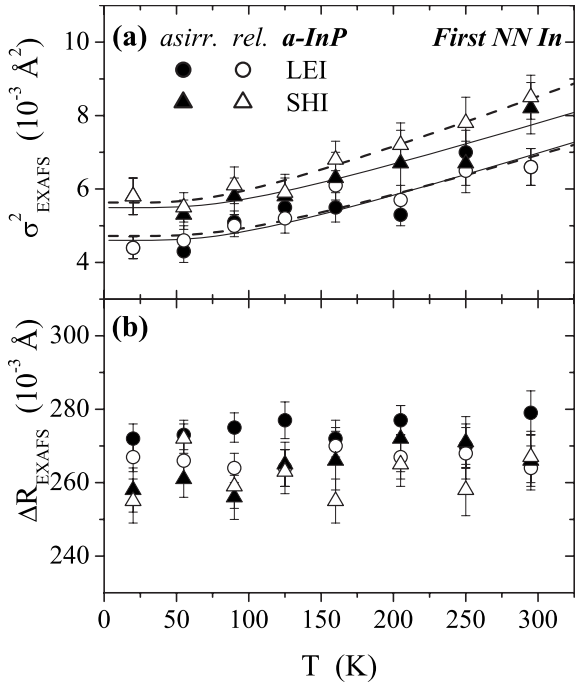

FIG. 9. (a) Debye-Waller factor $\sigma^2_{\mathrm{EXAFS}}$ and (b) interatomic distance $\Delta R_{\mathrm{EXAFS}}=R_{\mathrm{EXAFS}}(T)-2.541$ Å versus temperature T for first NN In a-InP. LEI and SHI samples are plotted as circles and triangles, respectively. Full symbols represent the as-irradiated phase whereas open symbols give the parameters obtained after relaxation. The lines show the corresponding Einstein model fits.

in Table III and discussed above, they are much closer to each other (~370–390 K) than to the value obtained from $\mathrm{MSD}_{\mathrm{In+P}}$ (~170 K). Similarly, $E_\parallel$ for the first NN In-In pairs of the amorphous samples is much higher than the value for $\mathrm{MSD}_{\mathrm{In+In}}$ (~260 K compared to ~110 K, respectively). If we assume the MSDs for both phases are of a similar order, then vibrations of first NN atoms along the bond direction in the amorphous material must be correlated in a manner similar to that observed for c-InP with a strong (but not complete) in-phase motion of the neighboring atoms.

Thus, comparing crystalline and amorphous phases, two main conclusions can be drawn: (i) the thermal behavior (i.e., $E_\parallel$, k_3) is similar for a-InP and c-InP whereas the structural disorder (i.e., $\sigma^2_{\mathrm{static},\parallel}$, $C_{3,\mathrm{static}}$) is much higher in the amorphous phase than in the crystalline one. (ii) Relative motion of first NN atoms parallel to the bond direction is reduced by a similar amount for a-InP and c-InP when compared to the crystalline MSD. We suggest that the bonding character and hence the interaction potential is similar for the two phases consistent with the observed thermal and vibrational behavior since atomic motion is determined by the energy required to stretch and bend these bonds.

V. CONCLUSION

The structural parameters of crystalline and amorphous InP have been determined by EXAFS measurements over a temperature range of 20–295 K. EXAFS is sensitive to the correlated motion of the atoms and thus yields valuable insight into the phase relation of the atomic vibrations. Furthermore, by comparing XRD and EXAFS measurements one can distinguish between vibrations parallel and perpendicular to the bond direction. For c-InP, a strong vibrational anisotropy is observed where relative vibrations parallel to the bond are significantly smaller than the uncorrelated MSD determined by XRD while relative vibrations perpendicular to the bond are very similar. This is consistent with a strong (but not complete) in-phase motion of the neighboring atoms along the bond direction and mostly uncorrelated vibrations perpendicular to it. Such behavior can be understood by considering the energy required for the two types of motion: relative vibrations along the bond require bond stretching while relative vibrations perpendicular to the bond mainly change the bond angle and thus involve bond bending. For III-V semiconductors with the zinc-blende structure, bond bending is energetically favored over bond stretching with the ratio of the corresponding force constants being ~1/6. A similar factor is obtained in the present study when comparing the force constants for relative vibrations perpendicular and parallel to the bond direction. The correlation of vibrations along the line of absorber-backscatterer pairs strongly decreases for the higher NN shells due to the fact that changes in the bond angles do alter the higher NN distances even if the first NN bond length remains unchanged. For the third NN shell, the amplitude of relative vibrations along the line of the two atoms already approaches the uncorrelated MSD. For a-InP, a strong increase in structural disorder is observed compared to c-InP; however, the temperature-

TABLE III. Einstein temperature $E_\parallel$ and static contribution to the Debye-Waller factor $\sigma^2_{\mathrm{static},\parallel}$ as determined from fits with a correlated Einstein model for the first NN shell of c-InP and a-InP. Anharmonic constant k_3 and static contribution to the third cumulant $C_{3,\mathrm{static}}$ are also given for the In-P pairs.

		First NN In-P				First NN In-In	
		$E_\parallel$ (K)	$\sigma^2_{\mathrm{static},\parallel}$ (10^{-3} Å^2)	k_3 (kg Å^{-1} s^{-2})	$C_{3,\mathrm{static}}$ (10^{-5} Å^3)	$E_\parallel$ (K)	$\sigma^2_{\mathrm{static},\parallel}$ (10^{-3} Å^2)
c-InP		392 ± 8	0.0 ± 0.2	120 ± 30	−1 ± 7		
a-InP SHI	As-irrad.	370 ± 10	3.1 ± 0.2	230 ± 50	22 ± 6	260 ± 20	3.9 ± 0.3
	Relaxed	382 ± 10	2.6 ± 0.2	200 ± 50	19 ± 6	240 ± 20	3.9 ± 0.3
a-InP LEI	As-irrad.	369 ± 10	3.1 ± 0.2	150 ± 50	25 ± 6	260 ± 20	3.0 ± 0.3
	Relaxed	384 ± 10	2.9 ± 0.2	150 ± 50	21 ± 6	270 ± 20	3.1 ± 0.3

dependent behavior and thus the thermally induced disorder is very similar for both phases. Furthermore, a strong reduction in first NN relative vibrations parallel to the bond is likely, similar to what is observed for *c*-InP. We suggest the similarities in vibrational behavior of crystalline and amorphous InP stem from the fact that the bonding character is similar for the two phases despite their difference in structure.

ACKNOWLEDGMENTS

We thank H. H. Tan for the growth of the $InP/In_{0.53}Ga_{0.47}As/InP$ heterostructures. We also thank the staff at the ANU Heavy-Ion Facility and at beam line NW10A of the Photon Factory for their continued work and effort. The authors were supported by the Australian Synchrotron Research Program. P.K., A.P.B., and M.C.R. further acknowledge the support of the Australian Research Council.

[1] G. Dalba, P. Fornasini, R. Gotter, and F. Rocca, Phys. Rev. B **52**, 149 (1995).

[2] P. Fornasini, S. a Beccara, G. Dalba, R. Grisenti, A. Sanson, M. Vaccari, and F. Rocca, Phys. Rev. B **70**, 174301 (2004).

[3] G. Beni and P. M. Platzman, Phys. Rev. B **14**, 1514 (1976).

[4] E. Sevillano, H. Meuth, and J. J. Rehr, Phys. Rev. B **20**, 4908 (1979).

[5] G. Bunker, Nucl. Instrum. Methods Phys. Res. **207**, 437 (1983).

[6] A. I. Frenkel and J. J. Rehr, Phys. Rev. B **48**, 585 (1993).

[7] G. Dalba and P. Fornasini, J. Synchrotron Radiat. **4**, 243 (1997).

[8] G. Dalba, P. Fornasini, R. Grisenti, and J. Purans, Phys. Rev. Lett. **82**, 4240 (1999).

[9] T. Yokoyama, J. Synchrotron Radiat. **6**, 323 (1999).

[10] P. Fornasini, F. Monti, and A. Sanson, J. Synchrotron Radiat. **8**, 1214 (2001).

[11] M. Vaccari and P. Fornasini, J. Synchrotron Radiat. **13**, 321 (2006).

[12] A. Filipponi and A. Di Cicco, Phys. Rev. B **51**, 12322 (1995).

[13] G. Dalba, P. Fornasini, M. Grazioli, and F. Rocca, Phys. Rev. B **52**, 11034 (1995).

[14] G. Dalba, D. Diop, P. Fornasini, and F. Rocca, J. Phys.: Condens. Matter **6**, 3599 (1994).

[15] G. Dalba, P. Fornasini, R. Grisenti, D. Pasqualini, D. Diop, and F. Monti, Phys. Rev. B **58**, 4793 (1998).

[16] G. Dalba, P. Fornasini, F. Rocca, and S. Mobilio, Phys. Rev. B **41**, 9668 (1990).

[17] C. S. Schnohr, P. Kluth, A. P. Byrne, G. J. Foran, and M. C. Ridgway, Phys. Rev. B **77**, 073204 (2008).

[18] G. de M. Azevedo, C. J. Glover, M. C. Ridgway, K. M. Yu, and G. J. Foran, Phys. Rev. B **68**, 115204 (2003).

[19] M. C. Ridgway, C. J. Glover, G. de M. Azevedo, S. M. Kluth, K. M. Yu, and G. J. Foran, Nucl. Instrum. Methods Phys. Res. B **238**, 294 (2005).

[20] L. L. Araujo, P. Kluth, G. de M. Azevedo, and M. C. Ridgway, Phys. Rev. B **74**, 184102 (2006).

[21] M. Newville, J. Synchrotron Radiat. **8**, 322 (2001).

[22] B. Ravel and M. Newville, J. Synchrotron Radiat. **12**, 537 (2005).

[23] A. L. Ankudinov, B. Ravel, J. J. Rehr, and S. D. Conradson, Phys. Rev. B **58**, 7565 (1998).

[24] Floating S_0^2 and E_0 for each measured temperature gave only a slight variation in the values significantly smaller than the experimental uncertainty, and showed no trend with temperature. Hence, the parameters were fixed to average values, similar to the analysis of Sanson *et al.* in Ref. 31, yielding $S_0^2=1.00$ and $E_0=9.2$ eV consistent with our previous measurements.

[25] Relating the relative increase $\Delta R_{\mathrm{EXAFS}}/R_{\mathrm{EXAFS}}$ of the first and second shells to each other or to the relative lattice expansion, $(R_C-R_0)/R_0$, is far from trivial since R_{EXAFS} depends on the crystallographic distance R_C and on the relative vibrations perpendicular to the line connecting absorber-backscatterer pair ($R_{\mathrm{EXAFS}}=R_C+\mathrm{MSRD}_\perp/2R_0$). The relative lattice expansion, $(R_C-R_0)/R_0$, is the same for all coordination shells. In contrast, the $\mathrm{MSRD}_\perp$ may be different for first and second NN shells due to a different correlation in the absorber-backscatter motion, as is indeed observed for $\mathrm{MSRD}_\parallel=\sigma^2_{\mathrm{EXAFS}}$ [see Fig. 5(a)]. In fact, we have exploited this very difference between R_{EXAFS} and R_C to obtain information about the $\mathrm{MSRD}_\perp$ for the first NN shell (see Figs. 6 and 7). Given the strong correlation between $R^{(2)}_{\mathrm{EXAFS}}$ and $C_3^{(2)}$, the large uncertainties of the values, and the dependence of the results on the fitting protocol, no such analysis or physical interpretation is attempted for the second shell.

[26] P. Deus, H. A. Schneider, U. Voland, and K. Stiehler, Phys. Status Solidi A **103**, 443 (1987).

[27] W. Böhmer and P. Rabe, J. Phys. C **12**, 2465 (1979).

[28] R. Saravanan, S. K. Mohanlal, and K. S. Chandrasekaran, Z. Kristallogr. **200**, 7 (1992).

[29] J. S. Reid, Acta Crystallogr., Sect. A: Found. Crystallogr. **39**, 1 (1983).

[30] M. Schowalter, A. Rosenauer, J. T. Titantah, and D. Lamoen, Acta Crystallogr., Sect. A: Found. Crystallogr. **65**, 5 (2009).

[31] A. Sanson, F. Rocca, G. Dalba, P. Fornasini, R. Grisenti, M. Dapiaggi, and G. Artioli, Phys. Rev. B **73**, 214305 (2006).

[32] Sadao Adachi, *Physical Properties of III-V Semiconductor Compounds* (Wiley, New York, 1992).

[33] V. M. Glazov, A. S. Pashinkin, and L. M. Pavlova, High Temp. **40**, 369 (2002).

[34] C. S. Schnohr, L. L. Araujo, P. Kluth, D. J. Sprouster, G. J. Foran, and M. C. Ridgway, Phys. Rev. B **78**, 115201 (2008).

[35] P. N. Keating, Phys. Rev. **145**, 637 (1966).

[36] R. M. Martin, Phys. Rev. B **1**, 4005 (1970).

[37] A.-B. Chen and A. Sher, Phys. Rev. B **32**, 3695 (1985).

[38] M. C. Ridgway, C. J. Glover, K. M. Yu, G. J. Foran, C. Clerc, J. L. Hansen, and A. Nylandsted Larsen, Phys. Rev. B **61**, 12586 (2000).

[39] M. C. Ridgway, G. de M. Azevedo, C. J. Glover, K. M. Yu, and G. J. Foran, Nucl. Instrum. Methods Phys. Res. B **199**, 235 (2003).